9. Natsume A, Ishii D, Wakabayashi T, Tsuno T, Hatano H, Mizuno M, et al. IFN-beta down-regulates the expression of DNA repair gene MGMT and sensitizes resistant glioma cells to temozolomide. *Cancer Res* 2005;65:7573–9.
10. Natsume A, Wakabayashi T, Ishii D, Maruta H, Fujii M, Shimato S, et al. A combination of IFN-beta and temozolomide in human glioma xenograft models: implication of p53-mediated MGMT downregulation. *Cancer Chemother Pharmacol* 2007.
11. Aoki T, Takahashi JA, Ueba T, Oya N, Hiraoka M, Matsui K, et al. Phase II study of nimustine, carboplatin, vincristine, and interferon-beta with radiotherapy for glioblastoma multiforme: experience of the Kyoto Neuro-Oncology Group. *J Neurosurg* 2006;105:385–91.
12. Hatano N, Wakabayashi T, Kajita Y, Mizuno M, Ohno T, Nakayashiki N, et al. Efficacy of post operative adjuvant therapy with human interferon beta, MCNU and radiation (IMR) for malignant glioma: comparison among three protocols. *Acta Neurochir* 2000;142:633–8; discussion 9.
13. Watanabe T, Katayama Y, Yoshino A, Fukaya C, Yamamoto T. Human interferon beta, nimustine hydrochloride, and radiation therapy in the treatment of newly diagnosed malignant astrocytomas. *J Neurooncol* 2005;72:57–62.
14. Yoshida J, Kajita Y, Wakabayashi T, Sugita K. Long-term follow-up results of 175 patients with malignant glioma: importance of radical tumour resection and postoperative adjuvant therapy with interferon, ACNU and radiation. *Acta Neurochir* 1994;127:55–9.

Biochemical and Biophysical Research Communications 369 (2008) 1041–1046

Contents lists available at ScienceDirect

Biochemical and Biophysical Research Communications

journal homepage: www.elsevier.com/locate/ybbrc

Increased expression of highly sulfated keratan sulfate synthesized in malignant astrocytic tumors

Yukinari Kato [a,*,1], Norihito Hayatsu [a,b,1], Mika Kato Kaneko [a], Satoshi Ogasawara [a], Tetsutaro Hamano [c], Satoru Takahashi [b], Ryo Nishikawa [d], Masao Matsutani [d], Kazuhiko Mishima [d], Hisashi Narimatsu [a,b]

[a] Research Center for Medical Glycoscience (RCMG), National Institute of Advanced Industrial Science and Technology (AIST), Open Space Laboratory C-2, 1-1-1, Tsukuba, Ibaraki 305-8568, Japan
[b] Graduate School of Comprehensive Human Sciences, University of Tsukuba, 1-1-1 Tennodai, Tsukuba, Ibaraki 305-8575, Japan
[c] Hamano Statistical Analysis Office 6-7-15, Chuo-cho, Higashikurume-shi, Tokyo 203-0054, Japan
[d] Saitama Medical University International Medical Center 1397-1 Yamane Hidaka-shi, Saitama 350-1298, Japan

ARTICLE INFO

Article history:
Received 20 February 2008
Available online 7 March 2008

Keywords:
Keratan sulfate
Proteoglycan
Glycogene
Astrocytic tumor
Glioblastoma

ABSTRACT

Keratan sulfate (KS) proteoglycans are expressed on a subpopulation of microglia in normal adult brain. We previously showed the up-regulated expression of KS in one of glioblastoma cell lines using anti-KS antibody (5D4). However, it has not been clarified whether KS is expressed in brain tumors and is involved in their malignancy. In this study, 54 astrocytic tumors were investigated about KS-expression using Western-blot with 5D4. In six of 14 anaplastic astrocytomas (43%) and 23 of 34 glioblastomas (68%), KS was detected by 5D4. KS was hardly detected by 5D4 in diffuse astrocytoma, suggesting that KS-expression is significantly expressed in malignant astrocytic tumors. In immunohistochemistry, KS is highly expressed in cell surface of malignant astrocytic tumors. Taken together, KS might be associated with the malignancy of astrocytic tumors, and be useful for a prognostic factor of astrocytic tumors.

Keratan sulfate (KS) proteoglycans (KSPGs) consist of different core proteoglycans that are individually glycosylated to varying degrees with keratan sulfate chains [1]. Theses keratan sulfates are known to be inhibitory to axonal growth. During development, sulfated keratans are temporally and spatially located in areas in which restricted axonal growth occurs. In the adult, KS is also found on a subpopulation of microglia throughout the brain; however, KS was not detected on astrocyte or oligodendrocyte [2]. KS consists of a linear polymer of *N*-acetyllactosamine, Galβ1-4GlcNAcβ1-3, which is sulfated at the C-6 positions of galactose (Gal) and *N*-acetylglucosamine (GlcNAc) [1]. Elongation of the carbohydrate backbone of KS chain is catalyzed by enzymes of two glycosyltransferase families: β1,3-*N*-acetylglucosaminyltransferase (β3GnT) and β1,4-galactosyltransferase (β4GalT). Sulfation of the chain is catalyzed by two carbohydrate sulfotransferases. Recent reports have described enzymes which are involved in KS synthesis [3–9]. Keratan sulfate Gal-6-sulfotransferase (KSGal6ST) is for sulfation of Gal. In addition, *N*-acetylglucosamine-6-*O*-sulfotransferase (GlcNAc6ST)-1 and GlcNAc6ST-5 (also known as CGn6ST) are responsible for sulfation of *N*-acetylglucosamine.

Astrocytic tumors are the most common tumors of the central nervous system (CNS) and are categorized into diffuse astrocytomas (World Health Organization (WHO) Grade II), anaplastic astrocytomas (AA; WHO Grade III) and glioblastomas (GBM; WHO Grade IV) [10]. Despite advances in surgical techniques, radiation therapy, and adjuvant chemotherapy, their prognoses remain poor: the median survival time for patients with GBMs is only one year [11]. Glioblastoma may occur de novo or may result from progression of low-grade astrocytomas [12]. Molecular mechanisms of tumorigenesis and malignant progression are associated with the inactivation of tumor suppressor genes such as p53-Rb pathway or the overexpression of oncogenes such as epidermal growth factor receptor (EGFR) [13]. However, the mechanisms of tumorigenesis and progression of astrocytic tumors have not been resolved completely. Identification of glycogenes or glycans that are expressed differentially in high-grade astrocytomas, low-grade tumors or normal brain tissues is important to elucidate the molecular mechanisms of tumorigenesis and to develop novel therapeutic strategies.

In our recent study, we investigated the KS expression in glioblastoma cell lines using a monoclonal anti-KS antibody (5D4) and revealed KS is highly expressed in one of glioblastoma cell lines, LN229 [14]. Furthermore, we investigated the relationship

Abbreviations: KS, keratan sulfate; KSPGs, KS proteoglycans; Gal, galactose; GlcNAc, *N*-acetylglucosamine; KSGal6ST, keratan sulfate Gal-6-sulfotransferase; GlcNAc6ST, *N*-acetylglucosamine-6-*O*-sulfotransferase; β3GnT, β1,3-*N*-acetylglucosaminyltransferase; β4GalT, β1,4-galactosyltransferase.

* Corresponding author. Fax: +81 29 861 3191.
E-mail address: yukinari-k@bea.hi-ho.ne.jp (Y. Kato).

[1] These authors contributed equally to this work.

0006-291X/$ - see front matter © 2008 Elsevier Inc. All rights reserved.
doi:10.1016/j.bbrc.2008.02.130

between expression of KS and glycogenes that are involved in KS synthesis using quantitative real-time PCR, and showed clearly that LN229 expresses a high level of KSGal6ST. However, it has not been clarified whether KS is expressed in astrocytic tumors and is involved in their malignancy. In this study, we investigated the KS-expression in astrocytic tumors of various malignancies using Western-blot and immunohistochemistry with 5D4, and discussed whether KS-expression is associated with the malignancy of astrocytic tumors.

Materials and methods

Tissue samples. Tumor specimens were obtained during surgery from six patients with diffuse astrocytomas, 14 patients with anaplastic astrocytomas, and 34 patients with glioblastomas. Informed consent had been obtained previously from patients or their guardians. Tissue microarrays of astrocytic tumors were purchased from Cybrdi, Inc. (Frederick, MD). The histology of these tissue samples was confirmed by experienced neuropathologists.

Western-blot analysis. The tissues were lysed with lysis buffer (25 mM Tris (pH 7.4), 50 mM NaCl, 0.5% Na deoxycholate, 2% nonidet P-40, 0.2% SDS, 1 mM phenylmethylsulfonyl fluoride, and 50 mg/ml aprotinin) including protease inhibitor solution. Samples of the supernatant fraction were collected after centrifuging at 15,000*g* for 30 min. Four micrograms of the proteins were electrophoresed under reducing conditions on 10% polyacrylamide gel (Atto Bioscience, Tokyo, Japan). The separated proteins were transferred to a PVDF membrane. After blocking with 3% skim milk in PBS, the membrane was incubated with 5D4 (1/5000 dilution; Seikagaku Corp., Tokyo, Japan) or anti-β-actin antibody (1/5000 dilution; Sigma, St. Louis, MO), and subsequently with peroxidase-conjugated anti-mouse antibodies (1/5000 dilution; Bio-Rad Laboratories Inc., Hercules, CA). It was then developed for 1 min with ECL reagents (Amersham Pharmacia Biotech Inc.) using Amersham Hyperfilm ECL (Amersham Pharmacia Biotech Inc.).

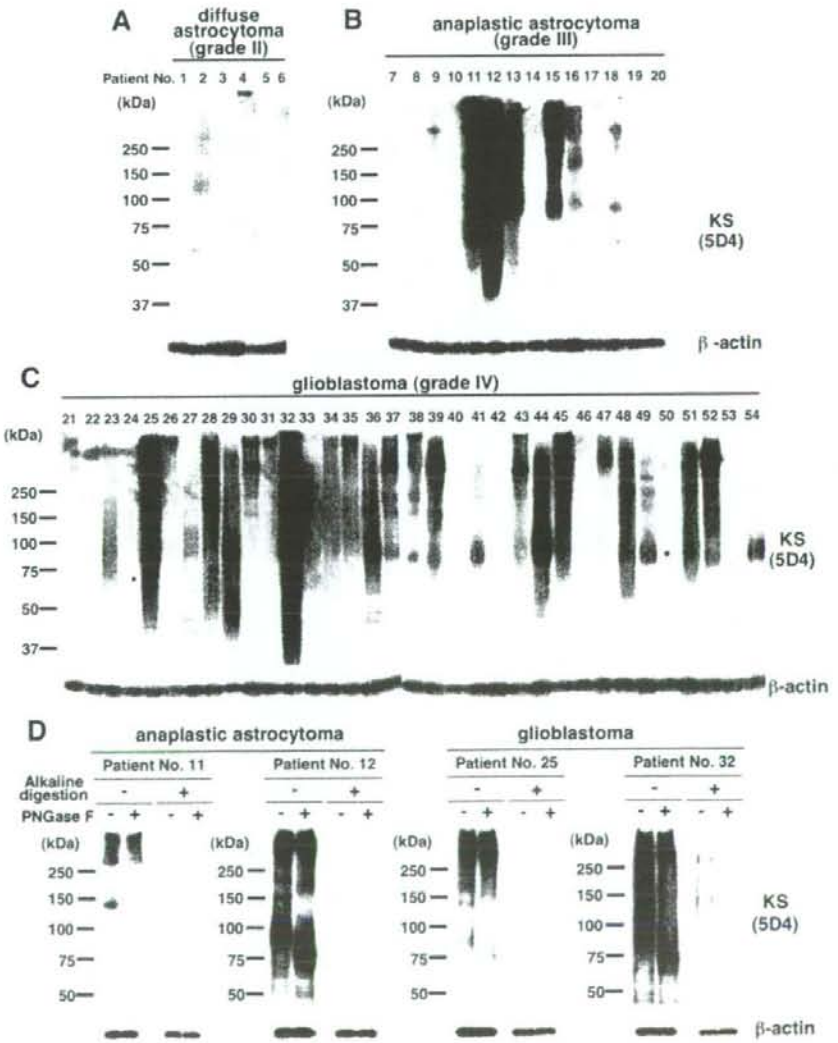

Fig. 1. Analysis of KS-expression in astrocytic tumors. Tissues from diffuse astrocytomas (A: lanes 1–6), anaplastic astrocytomas (B: lanes 7–20), and glioblastomas (C: lanes 21–54) were solubilized and immunoblotted using 5D4 (upper panel) or anti-β-actin antibody (lower panel). (D) The tissue lysates (patient Nos. 11, 12, 25, and 32) after treatment with PNGase F were electrophoresed and transferred onto PVDF membranes. The membranes were treated with PBS (left panel) or 0.05 M NaOH (right panel), and immunoblotted with 5D4 or anti-β-actin.

Deglycosylation experiments. The tissue lysate was treated PNGase F (Takara Bio Inc., Shiga, Japan; 0.1 mU/μg of protein) for 24 h at 37 °C according to the manufacturer's instructions. Alkaline digestion of *O*-glycans on the Western-blot was performed as described [14]. Briefly, transferred membrane of tissue lysate was incubated with 0.05 N NaOH for 16 h at 40 °C, prior to probing with antibody.

Immunohistochemical analysis. Specimens were deparaffinized, rehydrated, and incubated first with 5D4 (1/1000 dilution) at room temperature for 1 h, then with biotin-conjugated secondary anti-mouse IgG antibody (Dako, Glostrup, Denmark) for 1 h, and finally with peroxidase-conjugated biotin–streptavidin complex (Vectastain ABC Kit; Vector Laboratories Inc., Burlingame, CA) for 1 h. Color was developed using 3,3-diaminobenzidine tetrahydrochloride tablet sets (Dako) for 3 min. KS-expression was assessed semi-quantitatively from the percentage of tumor cells with cytoplasmic/membrane staining: 0, no staining; +, <10%; ++, 10–50%; +++, >50%.

Quantitative real-time PCR analysis. Total RNAs were prepared from 53 astrocytic tumors (seven diffuse astrocytomas, 14 anaplastic astrocytomas, and 32 glioblastomas) using an RNeasy mini prep kit (Qiagen Inc., Hilden, Germany). The initial cDNA strand was synthesized using SuperScript III transcriptase (Invitrogen Corp., Carlsbad, CA) by priming nine random oligomers and an oligo-dT primer according to the manufacturer's instructions. Real-time PCR was carried out on a LightCycler 480 Instrument with 96-well unit (Roche, Mannheim, Germany), using the LightCycler 480 SYBR Green I Master (Roche). Sets of primers were designed online with Primer3 (http://frodo.wi.mit.edu). The PCR conditions were 95 °C for 5 min (1 cycle), followed by 45 cycles of 95 °C for 10 s, 65 °C for 20 s, 72 °C for 20 s. Subsequently, a melting curve program was applied with continuous fluorescence measurement. Standard curves for each glycogene and β-actin template were generated by serial dilution of the PCR products (1×10^8 copies/μl to 1×10^2 copies/μl). The expression levels of glycogenes were normalized by the total RNA.

Statistical analyses. Results are expressed as the means ± standard deviation. Student's *t*-test was used to determine significance among the groups. A value of $p < 0.05$ was considered significant.

Table 1
Results of keratan sulfate immunostaining in 78 patients with astrocytic tumors

Tumor type	No. of cases	KS immunostaining				Positive rate
		+++	++	+	–	
Diffuse astrocytoma	20	0	0	0	20	0.0%
Tissue microarray	20	0	0	0	20	0.0%
Anaplastic astrocytoma	27	3	2	2	20	25.9%
Surgical resection samples	3	1	0	0	2	33.3%
Tissue microarray	24	2	2	2	18	25.0%
Glioblastoma	31	5	6	8	12	61.3%
Surgical resection samples	13	3	1	6	3	76.9%
Tissue microarray	18	2	5	2	9	50.0%

Results

Analysis of KS expression in astrocytic tumors

Lysates of frozen tumor specimens from 54 patients (six diffuse astrocytomas, 14 anaplastic astrocytomas, and 34 glioblastomas) were analyzed using Western-blot analysis with monoclonal anti-KS antibody, 5D4, which recognize highly sulfated KS [15]. As shown in Fig. 1, 5D4 detected highly sulfated KS in extracts of anaplastic astrocytoma (Grade III) and glioblastoma (Grade IV). One of six diffuse astrocytomas (17%), six of 14 anaplastic astrocytomas (43%), and 23 of 34 glioblastomas (68%) were detected by 5D4: two of 14 anaplastic astrocytomas (14%) and four of 34 glioblastomas (12%) were detected strongly; two of 14 anaplastic astrocytomas (14%) and 10 of 34 glioblastomas (29%) were detected moderately. Only one of diffuse astrocytomas (17%) was de-

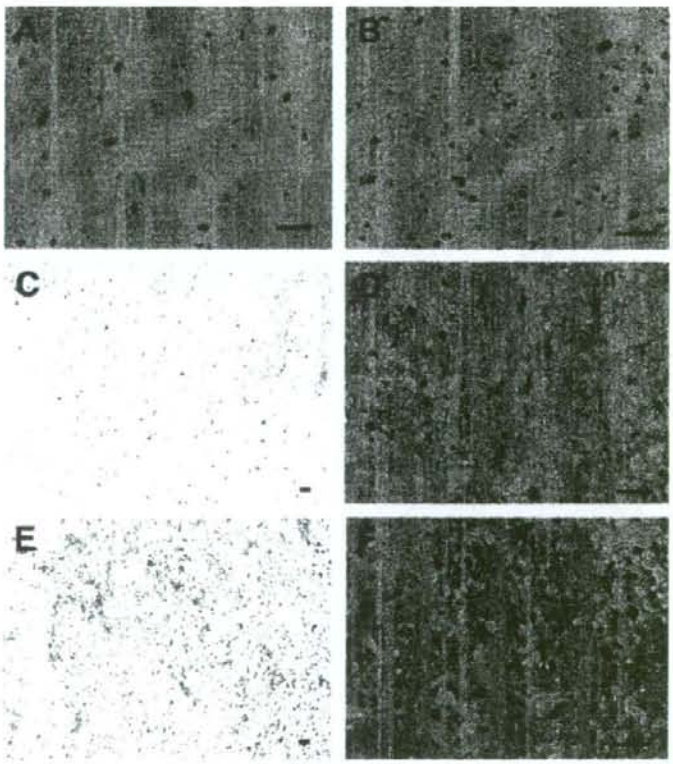

Fig. 2. Immunohistochemical detection of KS-containing proteoglycans in astrocytic tumors. No staining is apparent in a normal brain (A: 400×) and in diffuse astrocytoma (B: 400×). In anaplastic astrocytoma (patient No. 13), the tumor cell surface was stained positively (C: 100×, D: 400×). Accentuated staining is visible around an area of microvascular proliferation in glioblastoma (patient No. 32; E: 100x, F: 400x). Bar 10 μm.

tected weakly by 5D4. To determine whether 5D4-positive tissues express *N*-linked or *O*-linked KS, the tissue lysate was digested with PNGase F, then analyzed by Western-blot using 5D4. As depicted in Fig. 1D, the PNGase F treatment reduced some 5D4-positive signals. However, most signals were still observed. The PNGase F-undigested signals disappeared almost completely by sequential alkaline hydrolysis treatment to remove *O*-glycans (Fig. 1D), indicating that 5D4-positive tissues express both *N*-linked and *O*-linked KS.

Immunohistochemical staining for KS in malignant astrocytic tumors

The cellular distribution of KS in astrocytic tumors was examined immunohistochemically using 5D4. We used 62 tissues (20 diffuse astrocytomas, 24 anaplastic astrocytomas, and 18 glioblastomas) of tissue microarrays and 16 surgical tissues (three anaplastic astrocytomas and 13 glioblastomas) in immunohistochemistry. KS immunoreactivity was detected in seven of 27 (26%) anaplastic astrocytomas and in 19 of 31 (61%) glioblastomas; staining was graded as +++ in five glioblastoma and as ++ in six glioblastoma cases (Table 1). KS was not detected in diffuse astrocytomas. Representative staining for KS in astrocytic tumor samples is shown in Fig. 2. Immunostaining for KS demonstrated predominantly cell surface patterns. In anaplastic astrocytoma, the tumor cell surface was stained using 5D4, and the regional tendency was not observed (Fig. 2C and D). In glioblastomas, KS-positive tumor cells were prominent around microvascular proliferations (Fig. 2E and F). Proliferating endothelial cells were negative for KS (Fig. 2F). In non-neoplastic areas of the brain (Fig. 2A) and in diffuse astrocytoma (Fig. 2B), KS immunostaining was absent.

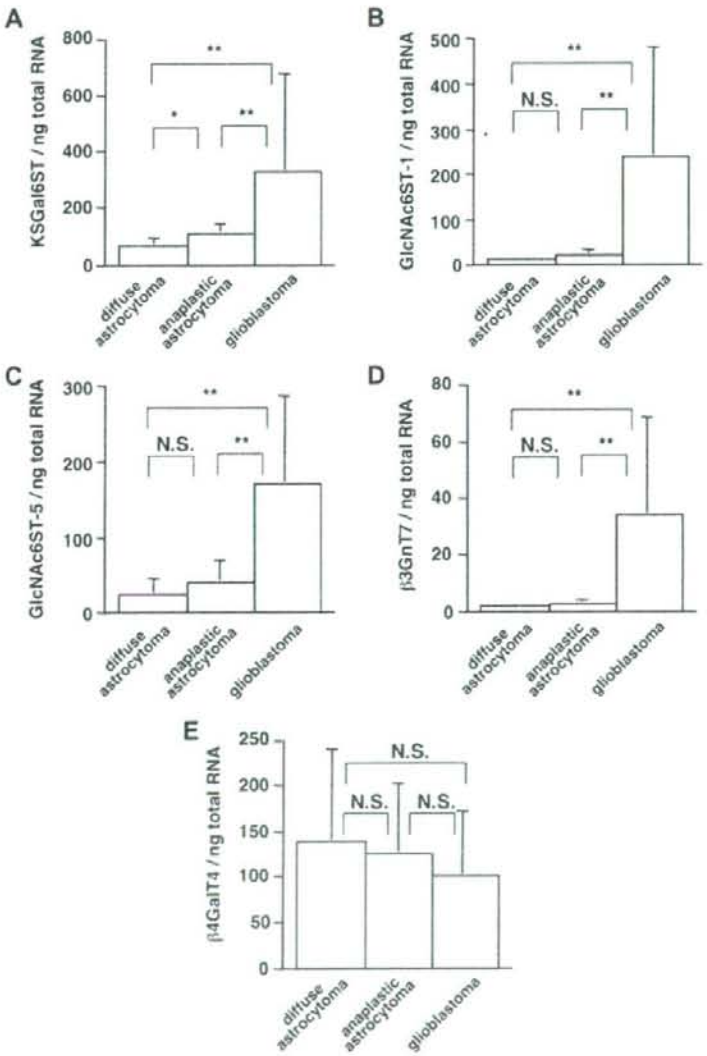

Fig. 3. Quantitative real-time PCR analysis of glycogenes for KS synthesis. The transcript levels for (A) KSGal6ST, (B) GlcNAc6ST-1, (C) GlcNAc6ST-5, (D) β3GnT7, and (E) β4GalT4 genes in 53 astrocytic tumors (seven diffuse astrocytomas, 14 anaplastic astrocytomas, and 32 glioblastomas) were measured using real-time PCR. Values normalized to the level of total RNA are presented. $^{**}p < 0.01$, $^{*}p < 0.05$.

Comparison of expression patterns of five genes involved in KS synthesis in astrocytic tumors

We performed quantitative real-time PCR analysis to compare the respective expression levels of five genes (KSGal6ST, GlcNAc6ST-1/-5, β3GnT7, and β4GalT4) involved in KS synthesis in 53 astrocytic tumors (seven diffuse astrocytomas, 14 anaplastic astrocytomas, and 32 glioblastomas). As shown in Fig. 3, the expression of KSGal6ST, GlcNAc6ST-1/-5, and β3GnT7 gradually increased associated with tumor malignancy. Comparing anaplastic astrocytoma with glioblastoma, the expression of KSGal6ST, GlcNAc6ST-1/-5, and β3GnT7 in glioblastoma is significantly higher than in anaplastic astrocytoma ($p < 0.01$). In comparison of diffuse astrocytoma with anaplastic astrocytoma, the expression of GlcNAc6ST-1 in anaplastic astrocytoma is significantly higher than in diffuse astrocytoma ($p < 0.05$). The expression of β4GalT4 has no significant difference among different grades of astrocytic tumors.

Discussion

Keratan sulfate (KS) is a glycosaminoglycan that is formed through the elongation of *N*-glycans or *O*-glycans attached covalently to scaffold proteins [1,16]. KS proteoglycans (KSPGs) are found in the extracellular matrix or cell surface in numerous tissues, predominantly in those of the cornea, cartilage, and brain. In the normal adult brain, KS expression is restricted to a subpopulation of microglia [2]. KS expression responds to embryonic development, physiological variations, and wound healing [1,16,17]. However, it has not been investigated whether KS is expressed in brain tumors and is further involved in malignant progression of brain tumors, especially astrocytic tumors.

In this study, lysates of frozen tumor specimens were analyzed using Western-blot analysis with monoclonal anti-KS antibody, 5D4 (Fig. 1). As a result, one of six diffuse astrocytomas (Grade II; 17%) and 29 of 48 high-grade astrocytic tumors (Grade III and IV; 60%) were detected by 5D4, indicating that highly sulfated KS-expression might be associated with its malignancy. Of high-grade astrocytic tumors, six of 14 anaplastic astrocytomas (43%) and 23 of 34 glioblastomas (68%) were detected by 5D4 ($p < 0.05$); therefore, there is significant difference about KS-expression between anaplastic astrocytomas and glioblastomas. We also investigated the KS expression in immunohistochemistry, and also showed the significant difference about KS expression between anaplastic astrocytomas (26%) and glioblastoma (61%; $p < 0.05$). We previously investigated the expression of podoplanin, which is associated with malignant progression of astrocytic tumors [18,19]. Podoplanin was expressed on the cell surface in 27% of anaplastic astrocytomas and 47% of glioblastomas using immunohistochemistry with anti-podoplanin antibody. On the other hand, podoplanin expression was not observed in diffuse astrocytomas. Furthermore, podoplanin expression is associated with poor prognosis of glioblastoma patients. Interestingly, KS-expression is highly associated with podoplanin expression in diffuse astrocytomas and anaplastic astrocytomas (data not shown), also suggesting that KS-expression might be involved in malignancy of astrocytic tumors.

In our recent study, we investigated how KS expression is regulated in glioblastoma cell lines [14]. We performed quantitative real-time PCR analysis in 10 glioblastoma cell lines to compare the respective expression levels of five glycogenes (KSGal6ST, GlcNAc6ST-1/5, β3GnT7, and β4GalT4), which are involved in KS synthesis; LN229 cells expressed high level of these five glycogenes, especially KSGal6ST. Knockdown of KSGal6ST in LN229 using siRNAs for KSGal6ST considerably reduced the 5D4-reactivity shown by Western-blot analysis. KSGal6ST-transfected LN464 cells express a higher level of highly sulfated KS than control LN464. In this study, we also performed quantitative real-time PCR analysis to compare the respective expression levels of five glycogenes involved in KS synthesis in 53 astrocytic tumors. Of five glycogenes, the expression of KSGal6ST, GlcNAc6ST-1/-5, and β3GnT7 gradually increased associated with tumor malignancy (Fig. 3). Interestingly, the expression of KSGal6ST, GlcNAc6ST-1/-5, and β3GnT7 in glioblastoma is significantly higher than in anaplastic astrocytoma. Moreover, the expression of GlcNAc6ST-1 in anaplastic astrocytoma is significantly higher than in diffuse astrocytoma, which is coincident with the high level of expression of KSGal6ST in LN229 glioblastoma cells [14]. These results suggest that glycogenes involved in KS synthesis increased in the malignant progression of astrocytic tumors, leading to the up-regulation of highly sulfated KS.

In summary, we revealed that KS significantly expressed in malignant astrocytic tumors, not in low-grade astrocytic tumors using Western-blot. In immunohistochemistry, KS is highly expressed in cell surface of tumor cells. Taken together, KS might be associated with the malignancy of astrocytic tumors, and be useful for a prognostic factor of astrocytic tumors. Further study is necessary to investigate how KS is involved in the invasion of astrocytic tumors or their malignant progression.

Acknowledgments

We thank Ms. Nana Matsuura for technical assistance. This study was supported in part by New Energy and Industrial Technology Development Organization (NEDO), by the Osaka Cancer Research Foundation (MK. Kaneko), by Mitsubishi Pharma Research Foundation (Y. Kato), by the YASUDA Medical Foundation (Y. Kato), and by the Inoue Foundation for Science (Y. Kato).

References

[1] J.L. Funderburgh, Keratan sulfate: structure, biosynthesis, and function, Glycobiology 10 (2000) 951–958.
[2] L.L. Jones, M.H. Tuszynski, Spinal cord injury elicits expression of keratan sulfate proteoglycans by macrophages, reactive microglia, and oligodendrocyte progenitors, J. Neurosci. 22 (2002) 4611–4624.
[3] M. Fukuta, J. Inazawa, T. Torii, K. Tsuzuki, E. Shimada, O. Habuchi, Molecular cloning and characterization of human keratan sulfate Gal-6-sulfotransferase, J. Biol. Chem. 272 (1997) 32321–32328.
[4] T. Torii, M. Fukuta, O. Habuchi, Sulfation of sialyl *N*-acetyllactosamine oligosaccharides and fetuin oligosaccharides by keratan sulfate Gal-6-sulfotransferase, Glycobiology 10 (2000) 203–211.
[5] T.O. Akama, A.K. Misra, O. Hindsgaul, M.N. Fukuda, Enzymatic synthesis in vitro of the disulfated disaccharide unit of corneal keratan sulfate, J. Biol. Chem. 277 (2002) 42505–42513.
[6] A. Seko, N. Dohmae, K. Takio, K. Yamashita, Beta 1,4-galactosyltransferase (beta 4GalT)-IV is specific for GlcNAc 6-O-sulfate. Beta 4GalT-IV acts on keratan sulfate-related glycans and a precursor glycan of 6-sulfosialyl-Lewis X, J. Biol. Chem. 278 (2003) 9150–9158.
[7] A. Seko, K. Yamashita, Beta1,3-*N*-Acetylglucosaminyltransferase-7 (beta3GnT7) acts efficiently on keratan sulfate-related glycans, FEBS Lett. 556 (2004) 216–220.
[8] H. Zhang, T. Muramatsu, A. Murase, S. Yuasa, K. Uchimura, K. Kadomatsu, *N*-Acetylglucosamine 6-O-sulfotransferase-1 is required for brain keratan sulfate biosynthesis and glial scar formation after brain injury, Glycobiology 16 (2006) 702–710.
[9] K. Kitayama, Y. Hayashida, K. Nishida, T.O. Akama, Enzymes responsible for synthesis of corneal keratan sulfate glycosaminoglycans, J. Biol. Chem. 282 (2007) 30085–30096.
[10] P. Kleihues, P.C. Burger, V.P. Collines, E.W. Newcomb, H. Ohagi, W.K. Cavenee, Astrocytic tumors. Glioblastama, International Agency for Research on Cancer Press, Lyons, France, 2000. pp. 29–39.
[11] L.M. DeAngelis, Brain tumors, N. Engl. J. Med. 344 (2001) 114–123.
[12] A. Giese, R. Bjerkvig, M.E. Berens, M. Westphal, Cost of migration: invasion of malignant gliomas and implications for treatment, J. Clin. Oncol. 21 (2003) 1624–1636.
[13] P. Kleihues, H. Ohgaki, Primary and secondary glioblastomas: from concept to clinical diagnosis, Neuro-oncology 1 (1999) 44–51.
[14] N. Hayatsu, S. Ogasawara, M.K. Kaneko, Y. Kato, H. Narimatsu, Expression of highly sulfated keratan sulfate synthesized in human glioblastoma cells, Biochem. Biophys. Res. Commun. 368 (2008) 217–222.

[15] H. Mehmet, P. Scudder, P.W. Tang, E.F. Hounsell, B. Caterson, T. Feizi, The antigenic determinants recognized by three monoclonal antibodies to keratan sulphate involve sulphated hepta- or larger oligosaccharides of the poly (*N*-acetyllactosamine) series, Eur. J. Biochem. 157 (1986) 385–391.
[16] H. Zhang, K. Uchimura, K. Kadomatsu, Brain keratan sulfate and glial scar formation, Ann. NY Acad. Sci. 1086 (2006) 81–90.
[17] R. Kleene, M. Schachner, Glycans and neural cell interactions, Nat. Rev. Neurosci. 5 (2004) 195–208.
[18] K. Mishima, Y. Kato, M.K. Kaneko, R. Nishikawa, T. Hirose, M. Matsutani, Increased expression of podoplanin in malignant astrocytic tumors as a novel molecular marker of malignant progression, Acta Neuropathol. (Berl) 111 (2006) 483–488.
[19] Y. Kato, M.K. Kaneko, A. Kuno, N. Uchiyama, K. Amano, Y. Chiba, Y. Hasegawa, J. Hirabayashi, H. Narimatsu, K. Mishima, M. Osawa, Inhibition of tumor cell-induced platelet aggregation using a novel anti-podoplanin antibody reacting with its platelet-aggregation-stimulating domain, Biochem. Biophys. Res. Commun. 349 (2006) 1301–1307.

Neurosurg Rev (2008) 31:165–172
DOI 10.1007/s10143-007-0103-7

ORIGINAL ARTICLE

Surgical treatment for choroid plexus tumors in the fourth ventricle: brain stem infiltration hinders total extirpation

Toshihiro Kumabe · Miki Fujimura · Hidefumi Jokura · Teiji Tominaga

Received: 25 May 2007 / Accepted: 18 August 2007 / Published online: 3 October 2007

Abstract The significance of surgery for choroid plexus tumors is well established, but surgical resection of those in the fourth ventricle has not been evaluated. This study reviewed five consecutive patients with choroid plexus tumors in the fourth ventricle treated in our institute between 1996 and 2005, focusing on the factors that hindered total extirpation. Two cases were choroid plexus papillomas, and three cases were choroid plexus carcinomas. Preoperative T2-weighted magnetic resonance imaging showed a diffuse high-intensity lesion in the brain stem in four patients. Infiltration into the fourth ventricle floor was apparent in all five patients during surgery, which hindered total resection of the tumors without neurological deterioration. Intraoperative bleeding was well controlled in all five patients by cauterizing the feeding arteries at the early stage of surgery through the telovelar approach. Performance status was improved in all patients postoperatively. All patients with choroid plexus carcinomas underwent radiation therapy after the surgical removal. No patient suffered tumor progression within the follow-up of 24–129 months (mean 64 months). Total resection of choroid plexus tumors in the fourth ventricle is difficult because of invasion into the fourth ventricle floor. Adjuvant therapy for choroid plexus tumors with brain stem infiltration must be established.

Keywords Brain stem · Choroid plexus carcinoma · Choroid plexus papilloma · Fourth ventricle · Invasion · Telovelar approach

T. Kumabe (✉) · M. Fujimura · T. Tominaga
Department of Neurosurgery,
Tohoku University Graduate School of Medicine,
1-1 Seiryo-machi, Aoba-ku,
Sendai 980-8574, Japan
e-mail: kuma@nsg.med.tohoku.ac.jp

M. Fujimura
e-mail: fujimur@nsg.med.tohoku.ac.jp

T. Tominaga
e-mail: tomi@nsg.med.tohoku.ac.jp

H. Jokura
Jiro Suzuki Memorial Gamma House,
Furukawa Seiryo Hospital,
Oosaki, Japan
e-mail: jokura@nsg.med.tohoku.ac.jp

Introduction

Choroid plexus tumors (CPTs) are rare intraventricular tumors accounting for about 0.4% of brain tumors according to the Brain Tumor Registry of Japan [19]. Choroid plexus papilloma (CPP) was as rare as 0.3% (147 cases), and malignant plexus papilloma (choroid plexus carcinoma; CPC) was even rarer with only 0.1% (29 cases) among 52,196 cases of brain tumor [19]. Only a few reports have described the treatment for this entity [1–3, 6, 8–12, 14–17, 20].

The extent of the surgical resection is widely accepted as the most important prognostic factor in patients with CPTs and particularly in patients with CPCs [3, 8, 9, 16, 17, 20]. However, total removal of CPC is achieved in as few as 36–64% of cases because of problems including intraoperative bleeding and infiltration of the normal brain structure [3, 8, 14–16]. More than 70% of patients with CPTs were under the age of 2 years [4, 6]. CPT is more common in the lateral ventricle in children but is more common in the fourth ventricle among adult patients [5, 19]. Surgical treatment for supratentorial CPTs has been discussed elsewhere [8, 14, 17], but that for fourth-ventricle CPTs has not been established.

Table 1 Clinical summary of five patients with choroid plexus

Case	Age	Sex	Pathology	Preoperative status	Preoperative MR imaging (high intensity in brain stem)	Resection	Postoperative MR imaging (residual-enhanced lesion)	Shunt	Radiation	Chemotherapy	Outcome at May 2007
1	28	M	CPP	KPS 90% truncal ataxia	Yes	1996/9/9 subtotal	Minute	None	None	None	KPS 100% progression-free
2	3	M	CPC	KPS 20% ICP↑ dysphagia dyspnea	Yes	2002/7/1 total	No	2002/6/21 ETV	WB and WS 24 Gy L 24 Gy	None	KPS 60% (elementary school life with gastrostoma, tracheotomy) progression-free
3	37	M	CPP	KPS100% no deficit	No	2002/9/19 subtotal	No	None	None	None	KPS 100% progression-free
4	25	F	CPC	KPS 50% ICP↑ truncal ataxia	Yes	2002/12/5 subtotal	Minute	None	WB and WS 30 Gy L 24 Gy	ACNU	KPS 100% progression-free
5	34	F	CPC	KPS 40% pregnancy ICP↑ vertigo	Yes	2005/6/20 partial	Yes	2005/5/23 ETV 2005/7/29 VPS	L 30 Gy, GK	None	KPS 90% (slight truncal ataxia, diplopia) progression-free

M Male, *F* female, *CPP* choroid plexus papilloma, *CPC* choroid plexus carcinoma, *KPS* Karnofski Performance Status, *ICP* intracranial pressure, *ETV* endoscopic third ventriculostomy, *VPS* ventriculo-peritoneal shunt, *WB* whole brain, *WS* whole spine, *L* local, *GK* gamma knife, *ACNU* nimustine hydrochloride

The present study reviewed our surgical experience with CPTs in the fourth ventricle, especially focusing on the problems regarding surgical resection.

Materials and methods

The present study included five consecutive patients, three male and two female aged 3 to 37 years, treated for CPTs in the fourth ventricle in our institute between 1996 and 2005. Two cases were CPPs, and three cases were CPCs. All patients with CPCs underwent radiation therapy after the surgical removal. A retrospective review of the case notes that pre- and postoperative magnetic resonance (MR) imaging, operation reports, and pathology was performed.

Surgical technique

All patients were operated on in the prone position. After suboccipital osteoplastic craniotomy and C-1 laminectomy, the dura was opened with a Y-shaped incision. The telovelar approach (transcerebellomedullary fissure approach) described previously [5, 7, 13] was applied to all cases. Any tumor protruding through the obex and/or the foramina of Luschka was initially removed using an Ultrasonic Surgical Aspirator (Sonopet; Miwatec, Tokyo, Japan) to expose and preserve the medulla oblongata, lower cranial nerves, and vascular structures including the vertebral arteries and posterior inferior cerebellar arteries (PICAs). The tela choroidea and inferior medullary velum were involved with the tumor in most of our cases. The concept of the surgery was as follows. The tela choroidea was incised along the taeniae choroidea with coagulation of the feeding arteries from the PICA to the tumor, to avoid damage to the branches to the brain stem. The inferior medullary velum was also incised. These procedures could reduce almost all of the blood supply to the tumor. Tumor debulking was then performed using the Ultrasonic Surgical Aspirator to expose and trace the normal fourth ventricle floor. Considerable care was taken to avoid injury to the fourth ventricle floor.

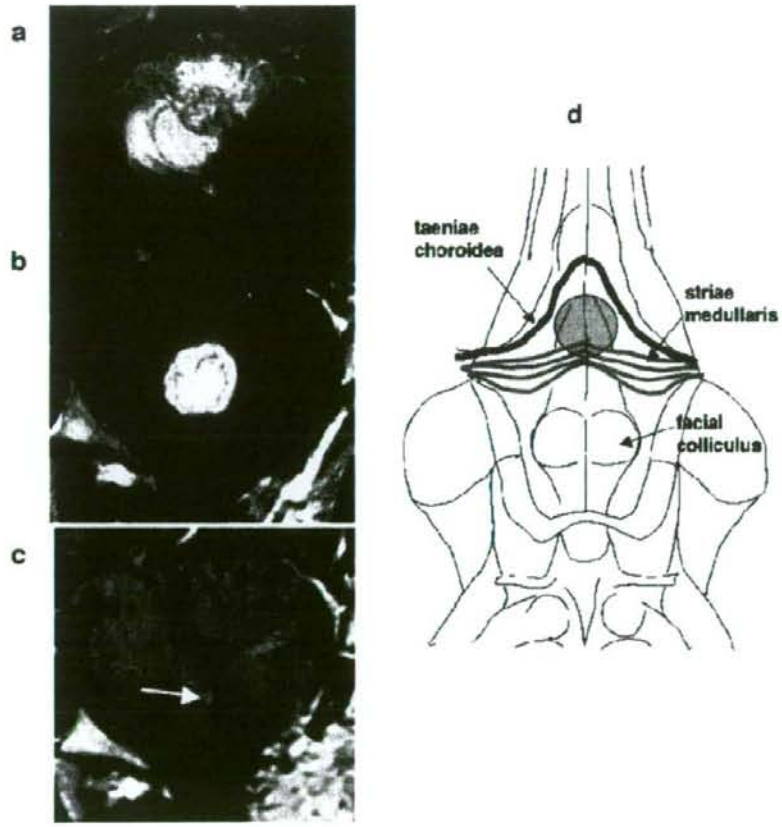

Fig. 1 Case 1, a 28-year-old man with choroid plexus papilloma. Axial T2-weighted magnetic resonance (MR) image showing the lesion associated with a high-intensity lesion in the adjacent neural tissue, including the brain stem (a). Sagittal T1-weighted MR image with gadolinium showing an enhanced mass with a cyst in the fourth ventricle (b). The tumor was removed subtotally, and the residual tumor was observed as an enhanced spot (c, *arrow*). Schematic drawing indicating invasion of the tumor into the fourth ventricle floor as the *shaded area* (d)

Results

Table 1 summarizes the clinical history, findings of MR imaging, and treatment of our five patients. Pre- and postoperative MR imaging and intraoperative findings are shown in Figs. 1, 2, 3, 4, and 5.

All patients except for case 3 (Fig. 3) had preoperative neurological deficits. Case 2 suffered severe dysphagia and respiratory disturbance because of infiltration of the tumor into the brain stem (Fig. 2). Three patients showed signs of high intracranial pressure because of obstructive hydrocephalus (Figs. 1, 4, and 5).

Preoperative T1-weighted MR imaging of all five patients demonstrated relatively well-demarcated lesions in the fourth ventricle enhanced by contrast material, whereas T2-weighted MR imaging showed a diffuse high-intensity lesion in the brain stem in four of the five cases (Figs. 1, 2, 4, and 5). Marked infiltration into the fourth ventricle floor was identified during surgery in these four cases, which hindered total resection of the tumors at the site of invasion. Brain stem invasion was also evident, to a lesser extent, in case 3 without high-intensity lesion in the brain stem on preoperative T2-weighted MR imaging (Fig. 3). The tumor had not always infiltrated into the brain stem at the site of taeniae choroidea, as brain stem infiltration occurred at the midline portion of the fourth ventricle floor in cases 1, 3, and 5 (Figs. 1, 3, and 5).

Total removal of the tumor was performed only in case 2 with CPC, who had already developed severe dysphagia and respiratory disturbance. Total resection of the tumor was planned preoperatively in this patient. Cases 1, 3, and 4 underwent subtotal removal, and case 5 underwent partial removal with maximum preservation of the normal brain stem structure. Postoperative MR imaging detected residual tumor in case 5 (Fig. 5) and small spot-enhanced nodules on the fourth ventricle floor in cases 1 and 4 (Figs. 1 and 4). Postoperative MR imaging showed no residual tumor in case 3, although the small amount of

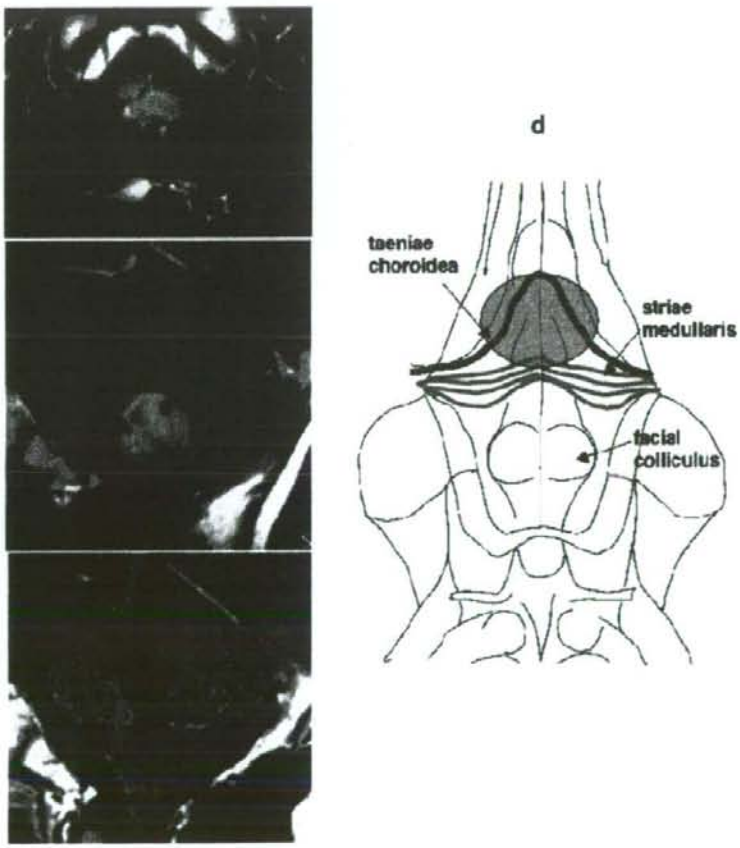

Fig. 2 Case 2, a 3-year-old boy with choroid plexus carcinoma. Axial T2-weighted magnetic resonance (MR) image disclosing the lesion associated with a high-intensity lesion in the adjacent neural tissue, including the brain stem (a). Sagittal T1-weighted MR image with gadolinium showing a dorsally exophytic enhanced mass within the medulla oblongata (b). The tumor was removed totally (c). Schematic drawing indicating invasion of the tumor into the hypoglossal and vagal trigone (d, *shaded area*)

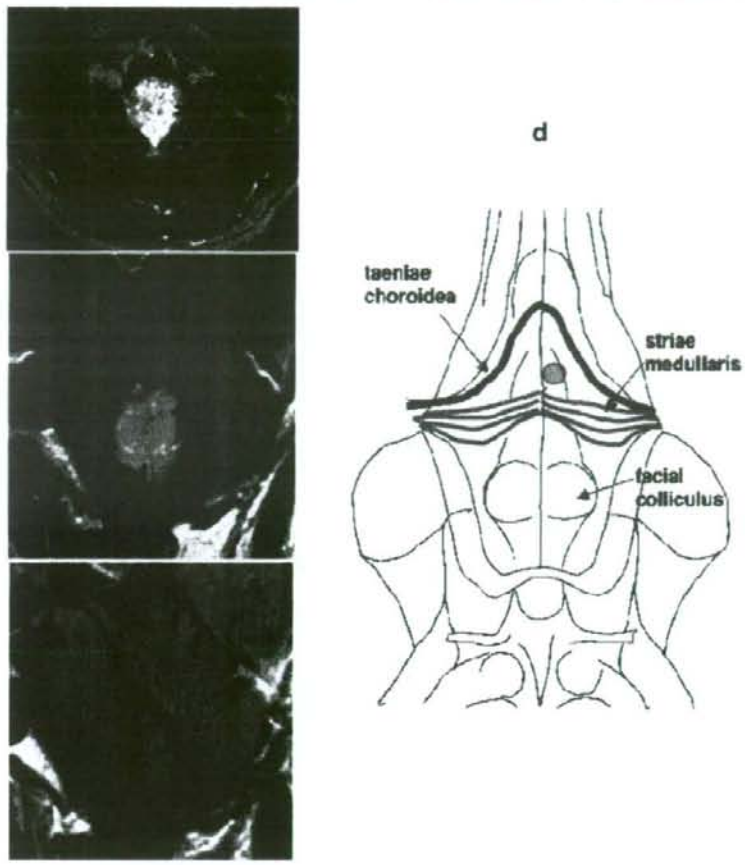

Fig. 3 Case 3, a 37-year-old man with choroid plexus papilloma. Axial T2-weighted magnetic resonance (MR) image showing the lesion but no associated high-intensity lesion in the adjacent neural tissue (a). Sagittal T1-weighted MR image with gadolinium showing an enhanced mass in the fourth ventricle (b). The tumor was removed almost totally, and no residual tumor was observed (c). However, intraoperative findings disclosed residual tumor on the fourth ventricle floor. Schematic drawing indicating tumor invasion into the fourth ventricle floor as the *shaded area* (d)

invasive tumor was left on the fourth ventricle floor (Fig. 3).

Intraoperative bleeding was well controlled in all five patients by cauterizing the tumor-feeding arteries at the early stage of surgery through the telovelar approach.

Performance status was improved in all patients postoperatively, and no patient had suffered tumor progression by May 2007, with a follow-up of 24 to 129 months (mean 64 months).

Illustrative case (case 5)

A 34-year-old woman in the 25th week of pregnancy was restricted to bed rest because of vertigo and nausea on admission. Preoperative T1-weighted MR imaging with contrast material demonstrated a well-delineated tumor with cystic formation in the fourth ventricle causing obstructive hydrocephalus and distortion of the brain stem (Fig. 5a and c). T2-weighted MR imaging disclosed the high-intensity lesion in the adjacent neural tissue, including the dorsal aspect of the brain stem (Fig. 5b). The patient initially underwent endoscopic third ventriculostomy for obstructive hydrocephalus, followed by successful cesarean section at the 30th week of pregnancy. Then, she underwent tumor removal by craniotomy. Surgical removal was extremely difficult because of the wide infiltration of the tumor into the fourth ventricle floor (Figs. 5f and g). The upper part of the tumor could not be resected because the normal fourth ventricle floor could not be traced above the striae medullaris (Fig. 5d). Adjuvant therapy using extended local irradiation and gamma knife stereotactic radiosurgery resulted in marked regression of the residual tumor (Fig. 5e). She was independent at the last follow-up, 2 years after the surgery. Her child is also doing well.

Discussion

The telovelar approach (transcerebellomedullary fissure approach) is one of the optimal surgical approaches for

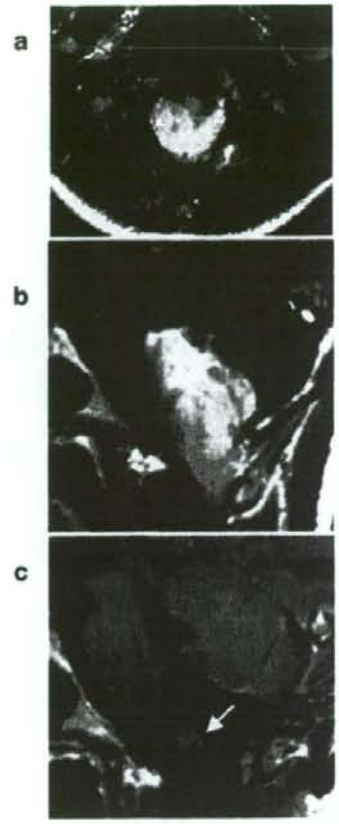

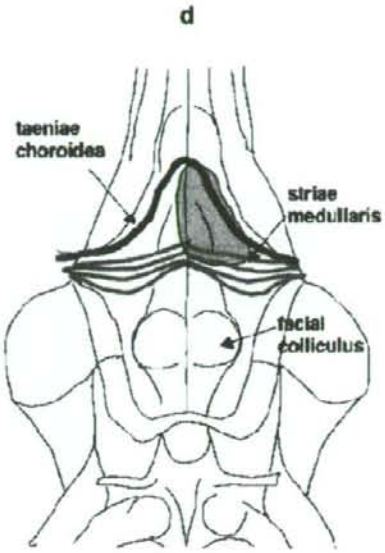

Fig. 4 Case 4, a 25-year-old woman with choroid plexus carcinoma. Axial T2-weighted magnetic resonance (MR) image disclosing the lesion associated with a high-intensity lesion in the medulla oblongata (a). Sagittal T1-weighted MR image with gadolinium showing an enhanced mass filling the fourth ventricle with extension into the cerebellomedullary fissure (b). The tumor was removed subtotally, and the residual tumor was observed as an enhanced lesion (c, *arrow*). Schematic drawing indicating tumor invasion into the fourth ventricle floor as the *shaded area* (d)

fourth-ventricle tumor [5, 7, 13]. This approach without splitting of the inferior vermis can avoid the development of cerebellar mutism syndrome. Because the blood supply to the choroid plexus in the fourth ventricle derives from the branch of PICA, the telovelar approach allows us to cauterize the feeding artery to the CPTs at the early stage of surgery. The advantage of this approach and the smaller size of CPTs in the fourth ventricle may together contribute to less intraoperative bleeding compared to CPTs in the lateral ventricle or the third ventricle. In the present series, intraoperative bleeding was well controlled in all five cases using this approach.

Infiltration into the fourth ventricle floor was apparent in all five cases during surgery. Anatomically, the attachment of the choroid plexus in the fourth ventricle is located at the side of ventricular wall and runs longitudinally along the midline, then passes laterally toward the bilateral lateral recesses [18], forming an inverted T-shape. The lateral parts of the choroid plexus extend to the bilateral cerebellopontine angles through the foramina of Luschka. Based on this anatomy, CPTs would not infiltrate the brain stem at the very beginning of the tumorigenesis. CPTs in the fourth ventricle may later infiltrate to the brain stem via the taeniae choroidea laterally or infiltrate directly through the fourth ventricle floor after a period of tumor adherence. CPCs are considered to be highly infiltrative, and this characteristic is a diagnostic indicator of CPCs. The present series demonstrated that both CPCs and CPPs may present with apparent infiltration into the fourth ventricle floor, which hinders total extirpation of the tumor during surgery. Tumor adherence to the floor of the fourth ventricle was encountered in one child with fourth ventricular papilloma, which necessitated subtotal removal [17]. Evidence of stromal invasion and/or focal brain invasion without other cellular changes may be clinically consistent with benign CPPs [12].

Therefore, we recommend preoperative evaluation of possible brain stem invasion by MR imaging in patients with suspected CPTs. Careful evaluation of the anatomical

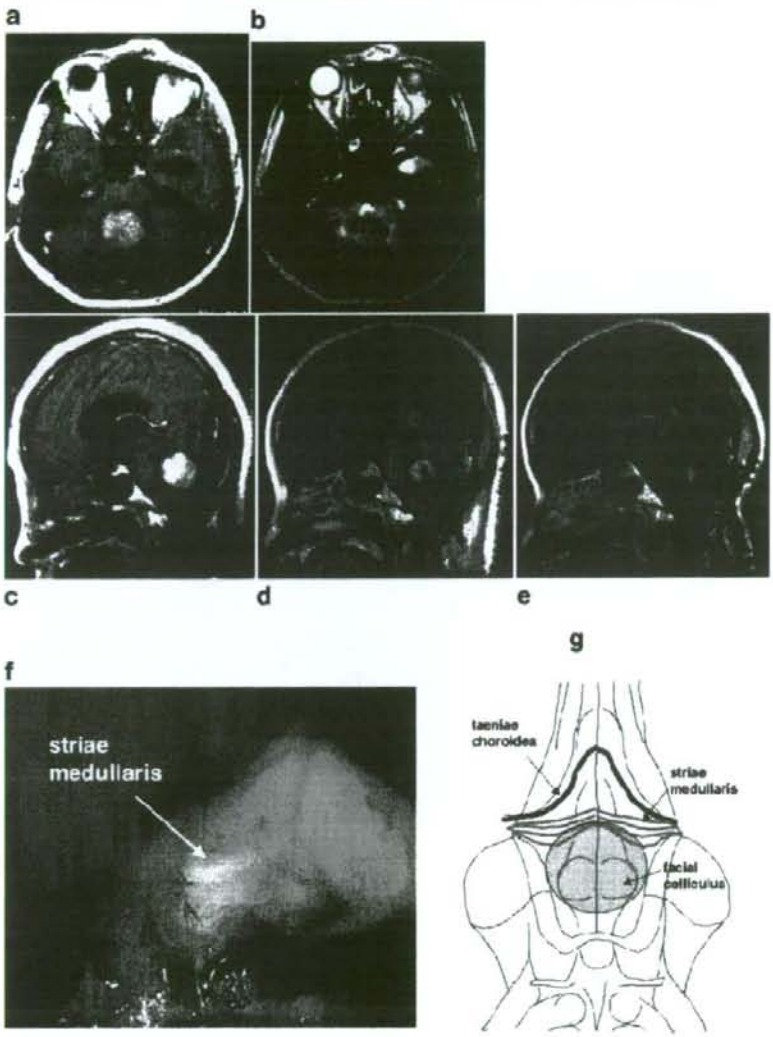

Fig. 5 Case 5, a 34-year-old woman with choroid plexus carcinoma. Axial (a) and sagittal (c) T1-weighted magnetic resonance (MR) images with gadolinium showing an enhanced mass with cystic formations filling the fourth ventricle. Axial T2-weighted MR image disclosing the lesion associated with a high-intensity lesion in the adjacent neural tissue, including the brain stem (b). The tumor was removed partially, and residual tumor was observed (d). Sagittal T1-weighted MR image with gadolinium obtained 1 year after extended local radiation and gamma knife stereotactic radiosurgery demonstrating shrinkage of the tumor (e). Intraoperative photograph after debulking of the tumor demonstrating the residual tumor invading the fourth ventricle floor (f). Schematic drawing indicating tumor invasion into the fourth ventricle floor as the *shaded area* (g)

relationship between the normal brain structure and the tumor, as well as the detection of the high-intensity lesion in the brain stem by T2-weighted MR imaging, may indicate the extent of brain stem invasion preoperatively.

The extent of surgical resection is generally accepted to be the most significant prognostic factor for CPCs [3, 8, 9, 16, 17, 20], but accurate histological diagnosis and evaluation of malignancy during surgery is not always possible to obtain. Such difficulties do not allow us to perform complete removal of the tumor, which may result in significant postoperative morbidity caused by destruction of the fourth ventricle floor. Therefore, we recommend removal of CPTs in the fourth ventricle as far as possible without affecting the normal brain stem structure. Complete surgical resection may be necessary for survival, and "second-look" procedures should be considered for patients who undergo subtotal resection [3, 8, 14]. If the lesion is localized and the patient's condition permits, most primary tumors of the choroid plexus should be removed completely via as many procedures as required, regardless of the size, site, and histological features [8]. However, total resection of CPTs in the fourth ventricle may be hindered by invasion into the fourth ven-

tricle floor, not by the excessive blood loss during surgery. Second-look surgery has the same risk of damage to the brain stem functions as the first surgery. Therefore, after the definitive histological diagnosis was established, we performed adjuvant radiochemotherapy for CPCs after discussion with a multidisciplinary team and also with the patients and family. We currently await the results of long-term follow-up of the patients with CPPs. The optimal postoperative treatment for the residual tumor in the fourth ventricle floor, including adjuvant radiochemotherapy or radiological follow-up without adjuvant therapy, is undetermined because of the limited number of patients with CPTs. The establishment of a worldwide registry for CPTs [9] would allow the development of a growing database of treatment strategies to address this critical issue.

Conclusion

The telovelar approach (transcerebellomedullary fissure approach) for CPTs in the fourth ventricle can control intraoperative bleeding by cauterizing the feeding arteries at the early stage of surgery. However, total resection is difficult because of infiltration into the brain stem. Future establishment of adjuvant therapy for CPTs with the brain stem infiltration is necessary to improve the prognosis.

References

1. Araki K, Aori T, Takahashi JA, Nozaki K, Nagata I, Kikuchi H, Yokoyama M, Hattori H, Akiyama Y, Kubota Y, Yokomizo H (1997) A case of choroid plexus carcinoma. No Shinkei Geka 25:853 857
2. Asai A, Hoffman HJ, Matsutani M, Takakura K (1991) Choroid plexus tumors in infancy. No Shinkei Geka 19:21 26
3. Berger C, Thiesse P, Lellouch-Tubiana A, Kalifa C, Pierre-Kahn A, Bouffet E (1998) Choroid plexus carcinomas in childhood: clinical features and prognostic factors. Neurosurgery 42:470 475
4. Boyd MC, Steinbok P (1987) Choroid plexus tumors: problems in diagnosis and management. J Neurosurg 66:800 805
5. Deshmukh VR, Figueiredo EG, Deshmukh P, Crawford NR, Preul MC, Spetzler RF (2006) Quantification and comparison of telovelar and transvermian approaches to the fourth ventricle. Neurosurgery 58: ONS 202-ONS-207
6. Dohrmann GJ, Collias JC (1975) Choroid plexus carcinoma. Case report. J Neurosurg 43:225 232
7. El-Bahy K (2005) Telovelar approach to the fourth ventricle: operative findings and results in 16 cases. Acta Neurochir (Wien) 147:137 142
8. Ellenbogen RG, Winston KR, Kupsky WJ (1989) Tumors of the choroid plexus in children. Neurosurgery 25:327 335
9. Fitzpatrick LK, Aronson LJ, Cohen KJ (2002) Is there a requirement for adjuvant therapy for choroid plexus carcinoma that has been completely resected? J Neurooncol 57:123 126
10. Kimura M, Takayasu M, Suzuki Y, Negoro M, Nagasaka T, Nakashima N, Sugita K (1992) Primary choroid plexus papilloma located in the suprasellar region: case report. Neurosurgery 31: 563 566
11. Kumabe T, Tominaga T, Kondo T, Yoshimoto T, Kayama T (1996) Intraoperative radiation therapy and chemotherapy for huge choroid plexus carcinoma in an infant. Neurol Med Chir (Tokyo) 36:179 184
12. Levy ML, Goldfarb A, Hyder DJ, Gonzales-Gomez I, Nelson M, Gilles FH, McComb JG (2001) Choroid plexus tumors in children: significance of stromal invasion. Neurosurgery 48:303 309
13. Matsushima T, Inoue T, Inamura T, Natori Y, Fukui M (2001) Transcerebellomedullary fissure approach with special reference to methods of dissecting the fissure. J Neurosurg 94:257 264
14. McEvoy AW, Harding BN, Phipps KP, Ellison DW, Elsmore AJ, Thompson D, Harkness W, Hayward RD (2000) Management of choroid plexus tumors in children: 20 years experience at a single neurosurgical centre. Pediatr Neurosurg 32:192 199
15. Noshita N, Kumabe T, Kayama T, Tominaga T (2006) Choroid plexus tumors: report of 7 cases in a single institution. No Shinkei Geka 34:73 81
16. Packer RJ, Perilongo G, Johnson D, Sutton LN, Vezina G, Zimmermann RA, Ryan J, Reaman G, Schut L (1992) Choroid plexus carcinoma of childhood. Cancer 69:580 585
17. Pencalet P, Sainte-Rose C, Lellouch-Tubiana A, Kalifa C, Brunelle F, Sgouros S, Meyer P, Cinalli G, Zerah M, Pierre-Kahn A, Renier D (1998) Papillomas and carcinomas of the choroid plexus in children. J Neurosurg 88:521 528
18. Rhoton AL Jr (2000) Cerebellum and fourth ventricle. Neurosurgery 47:S7 S27
19. The Committee of Brain Tumor Registry of Japan (2003) Report of brain tumor registry of Japan (1969 1996). Neurol Med Chir (Tokyo) 43(Suppl):36 43
20. Wolff JE, Sajedi M, Brant R, Coppes MJ, Egeler RM (2002) Choroid plexus tumours. Br J Cancer 87:1086 1091

Comments

Veit Rohde, Göttingen, Germany

The authors report five cases of CPT in the fourth ventricle. Only few larger series have been published so far, including patients with CPTs in the lateral and the third ventricles. The authors confirm again that papillomas as well as carcinomas invade brain tissue, here the floor of the fourth ventricle. Therefore, the authors did not try to remove the tumor completely to avoid neurological deficits. There was a progression-free survival after 64 months (mean), which supports the author's concept of a less aggressive surgical strategy. Using the telovelar approach, brisk bleeding could be controlled effectively. Even before this report, many neurosurgeons were reluctant to proceed to complete CPT removal in cases of infiltration of the fourth ventricular floor. Now, the neurosurgeons have the scientific justification for this strategy.

J Neurosurg 109:867–873, 2008

Convection-enhanced delivery of polyethylene glycol–coated liposomal doxorubicin: characterization and efficacy in rat intracranial glioma models

Laboratory investigation

Toshio Kikuchi, M.D.,[1] Ryuta Saito, M.D., Ph.D.,[1] Shin-ichirou Sugiyama, M.D.,[1] Yoji Yamashita, M.D., Ph.D.,[1] Toshihiro Kumabe, M.D., Ph.D.,[1] Michal Krauze, M.D.,[2] Krystof Bankiewicz, M.D., Ph.D.,[2] and Teiji Tominaga, M.D., Ph.D.[1]

[1]*Department of Neurosurgery, Tohoku University Graduate School of Medicine, Sendai, Miyagi, Japan; and* [2]*Department of Surgical Neurology, University of California, San Francisco, California*

Object. The characteristics of polyethylene glycol–coated liposomal doxorubicin (PLD), the only liposomal drug now clinically available for intravenous injection, were investigated after convection-enhanced delivery (CED) into the rat brain parenchyma.

Methods. The distribution, tissue retention, and toxicity profile were evaluated after CED into the rat brain parenchyma. The antitumor efficacy was also determined in rodent intracranial U-251MG and U-87MG glioma models.

Results. Convection-enhanced delivery of PLD achieved wider distributions and delayed onset of toxicity in the brain parenchyma compared with CED of free doxorubicin infusion. Fluorescence generated from doxorubicin infused as PLD was detected until at least 30 days after infusion. Local toxicity was not observed when a 10% dilution of the commercially available PLD solution was used (0.2 mg/ml doxorubicin), but was significant at higher concentrations. Results after 10% PLD was delivered locally with CED demonstrated significant survival prolongation in both intracranial U-251MG and U-87MG xenograft models.

Conclusions. Convection-enhanced delivery of PLD achieved extensive tissue distribution and sustained drug release. Convection-enhanced delivery of PLD is a promising chemotherapy for the treatment of malignant gliomas. *(DOI: 10.3171/JNS/2008/109/11/0867)*

Key Words • **chemotherapy** • **convection-enhanced delivery** • **glioma** • **liposomal doxorubicin** • **rat**

Chemotherapy for malignant gliomas remains a challenging field for researchers because of the chemoresistance often observed in these lesions.[4] Poor drug delivery is one explanation, caused by the hindrance of the blood–brain and blood–tumor barriers to the entry of chemotherapeutic agents administered systemically. Consequently, even in optimal situations, only a small fraction of the administered drug actually reaches the tumor cells. Local drug delivery is therefore a promising strategy for overcoming the chemoresistance of malignant glioma, as local administration results in 100% dose delivery to the target site. For example, Gliadel wafers (poly [carboxyphenoxy-propane/sebacic acid] anhydride wafers) are designed to release their 3.85% carmustine (1,3-bis-chlorethyl-1-nitrosourea) content slowly over a 2–3-week period after implantation on the surface of the tumor resection cavity. Authors of recent studies have demonstrated life-prolonging efficacy of Gliadel wafers against recurrent and primary malignant gliomas.[2,17] However, the major disadvantage to this method is the drug's limited distribution, as high-dose delivery occurs only within mm of the implant.[3] Therefore, a drug delivery method that achieves extensive distribution of the therapeutic agent together with slow-release capability may further improve the therapeutic efficacy.[12,13]

Convection-enhanced delivery is a relatively new drug delivery method that might overcome the problems of local drug delivery. This technique uses a pressure gradient established at the tip of an infusion catheter to create the bulk flow that pushes the drug through the interstitial space.[1]

Abbreviations used in this paper: CED = convection-enhanced delivery; PBS = phosphate-buffered saline; PLD = polyethylene glycol–coated liposomal doxorubicin.

We previously reported the efficacy of PLD delivered via CED in the rodent intracranial U-251MG glioma xenograft model.[18] Polyethylene glycol–coated liposomal doxorubicin is a liposomal drug approved for systemic intravenous delivery against breast cancer, ovarian cancer, and others.[8,10] Convection-enhanced delivery of PLD has been shown to be more effective than systemic delivery of the maximum tolerable dose, and CED of free doxorubicin.[18]

In the present study, we investigated the distribution, sustained release, and toxicity of PLD after CED in the normal rat brain parenchyma. Antitumor efficacy was also evaluated in the well-established rodent intracranial U-251MG and U-87MG xenograft models.[9]

Methods

Free Doxorubicin and PLD

Stock solutions of free doxorubicin (Sigma) were prepared by diluting the doxorubicin in dimethyl sulfoxide to a concentration of 50 mg/ml. The infusion solutions of free doxorubicin were made by diluting the stock solution with PBS. The infusion solution containing 4% dimethyl sulfoxide had no toxicity when 20 μl was infused by CED (data not shown). Polyethylene glycol–coated liposomal doxorubicin (Doxil [doxorubicin hydrochloride liposome], ALZA Corporation) was obtained commercially via iRxMedicine, Oz International Inc. The commercial PLD solutions contained 2 mg/ml of doxorubicin. The infusion solution was made by diluting the stock solution with PBS.

Tumor Cell Lines

The established human glioblastoma multiforme cell line, U-251MG, was obtained from the Brain Tumor Research Center Tissue Bank at the University of California, San Francisco. The U-87MG human glioblastoma cell line was purchased from the American Type Culture Collection. Cells were maintained as monolayers in a complete medium consisting of Eagle minimum essential medium supplemented with 10% fetal bovine serum and nonessential amino acids. Cells were cultured in an incubator at 37°C in a humidified atmosphere composed of 95% air and 5% carbon dioxide.

Experimental Animals

Seven-week-old male Fischer 344 rats were purchased from Japan SLC, Inc. Seven-week-old male Fischer 344/NJcl-rnu/rnu (nude) rats were purchased from CLEA Japan, Inc. Male Sprague–Dawley rats weighing ~ 250 g were obtained from Charles River Laboratories. Congenitally athymic, male nude rats (rnu/rnu, homozygous) weighing ~ 150–200 g were purchased from the National Cancer Institute. Protocols used in the animal studies were approved either by the Institute for Animal Experimentation, Tohoku University Graduate School of Medicine, or by the Institutional Animal Care and Use Committee, University of California, San Francisco.

Intracr

Cε n, washed once with complete medium, and suspended in Ca^{++}- and Mg^{++}-free PBS for implantation. A cell suspension containing 50×10^4 cells/10 μl in PBS was prepared for implantation. Fischer 344/NJcl-rnu/rnu (nude) rats were used for the U-87MG xenograft model, and nude rats (rnu/rnu, homozygous) were used for the U-251MG xenograft model. Under deep halothane anesthesia, the rats were placed in small-animal stereotactic frames (Narishige Co.). A sagittal incision was made through the skin to expose the cranium, and a bur hole was made with a small drill in the skull 0.5-mm anterior and 3-mm lateral to the bregma. At a depth of 4.5 mm from the brain surface, 5 μl of the cell suspension was injected. After 2 minutes, another 5 μl was injected at a depth of 4 mm and after another 2 minutes, the implantation needle was removed and the wound sutured.

Convection-Enhanced Delivery

The infusion was performed using the CED method as described previously.[11] A reflux-free infusion cannula consisting of a fine silica tube and a 27-gauge metal needle[6] was connected to the syringe placed on a microinfusion pump (BeeHive, Bioanalytical System) to control the infusion rate. The infusion proceeded at 0.2 μl/minute for 15 minutes, 0.5 μl/minute for 10 minutes, and 0.8 μl/minute for 15 minutes, for a total infusion 20 μl in 40 minutes. The therapeutic agent was infused locally at a 4.0-mm depth using the same stereotactic coordinates at 7 days after tumor implantation.

Detection of Doxorubicin

The drug distribution after CED was analyzed in 3 Fischer 344 rats that received 20 μl of 10% PLD (0.2 mg/ml doxorubicin) into the striatum. The rats were killed immediately after CED, and their brains harvested and frozen in dry ice–cooled isopentane. The fresh frozen brains were cut into 25-μm-thick coronal sections on a cryostat, and the sections were placed on microscope slides. Fluorescence generated from the doxorubicin with ultraviolet illumination was visualized under a fluorescent microscope and captured by a charge-coupled device camera (DFC350 FX, Leica Microsystems). To compare tissue distributions and toxicity onset after CED and PLD or free doxorubicin, 6 Sprague–Dawley rats received 100% PLD (2.0 mg/ml doxorubicin) in the right hemisphere and 2.0 mg/ml free doxorubicin in the left hemisphere. Three of these rats were killed 1 hour after infusion, and the other 3 were killed 5 days after infusion. The fresh frozen brains were observed under fluorescence and light microscopy.

Tissue Retention and Toxicity After CED

The clearance of PLD in rat brains was investigated in 8 normal Fischer 344 rats that received 20 μl of 10% PLD (0.2 mg/ml doxorubicin). Two rats were killed at 7, 14, 30, and 60 days after infusion, and their brains were processed for histological detection of fluorescence. The brain section with the highest fluorescence intensity was photographed with a charge-coupled device camera. The toxicity on normal brain parenchyma of the PLD delivered locally via CED was evaluated in 12 Fischer 344

rats divided into 4 groups according to type of 20-μl infusion: the sham surgery group received PBS, and the other 3 groups received 10% PLD (0.2 mg/ml doxorubicin), 20% PLD (0.4 mg/ml doxorubicin in concentration), or 100% PLD (2.0 mg/ml doxorubicin). Body weight was measured before CED and then weekly thereafter. Sixty-three days after CED, the rats were killed, perfused with 10% formalin, and the brains processed for histological examination with H & E staining.

Survival Study

Seven days after implantation, 12 rats with U-251MG tumor cells and 14 with U-87MG tumor cells were randomly divided into 2 groups: a sham surgery group that underwent CED of PBS (6 rats with U-251MG and 7 with U-87MG cells), and a group that underwent CED of 10% PLD (0.2 mg/ml doxorubicin; 6 rats with U-251MG and 7 with U-87MG cells). All rats were carefully observed for general health and survival.

Statistical Analysis

Animal survival was plotted using the Kaplan–Meier method. Differences in survival were determined using the log-rank test and probability values < 0.05 were considered statistically significant. Commercially available software (StatMate software, ATMS Co., Ltd.) was used for statistical analysis.

Results

Distribution of PLD in Brain Parenchyma

Effective distribution of PLD was confirmed in the rodent brain. Representative serial sections obtained at 1-mm intervals are shown in Fig. 1. Fluorescence generated from doxorubicin by ultraviolet illumination demonstrated extensive distribution of PLD after CED. Similar distributions were found in all 3 rats tested.

Tissue Distribution and Onset of Toxicity of PLD and Free Doxorubicin After CED

At 1 hour after infusion, slight damage to the brain at the site of the infusion was observed only in the left hemisphere that had received free doxorubicin. Distributions of PLD were much larger than those of free doxorubicin (Fig. 2A). Five days after infusion, severe local toxicity was found in the left hemisphere that had received free doxorubicin, whereas only slight tissue changes were found in right hemisphere that received PLD. Diffuse fluorescence from doxorubicin was found in the normal brain tissue surrounding the necrotic cavity of the hemisphere that had received free doxorubicin, probably causing more severe side effects. In contrast, in the hemisphere that received PLD the fluorescence remained mostly at the same site as observed within 1 hour of the infusion (Fig. 2B).

Tissue Retention of PLD After CED

Based on the late onset of toxicity found in the hemisphere that received PLD, we evaluated the duration of tissue retention of PLD using a 10% dilution of the stock solution (0.2 mg/ml doxorubicin). Fluorescence generated from doxorubicin by ultraviolet illumination was detected in rodent brains at 7, 14, 30, and 60 days after CED (Fig. 3). The signal intensity remained high until 14 days after CED, but then gradually decreased. Only faint fluorescence was detectable in the brain parenchyma by 60 days after infusion.

Toxicity of PLD in Normal Rodent Brain

Because the fluorescence generated from doxorubicin had diminished by 60 days after infusion, toxicity analysis was continued until 63 days after infusion. All rats that had received PLD in any concentration by CED gained body weight steadily at the same rate as the control rats until 63 days postinfusion (Fig. 4A). Daily observations also revealed no clinical deficits in all rats during the 63-day observation period. All rats were killed at 63 days after infusion of PLD, and their brains were processed (Fig. 4B). Histological examination revealed brain tissue damage in rat brains that received 0.4 mg/ml doxorubicin as PLD (20% dilution) or above. The 3 rats that received 0.2 mg/ml doxorubicin as PLD survived without clinical symptoms until 63 days after infusion, and brain tissue damage was almost negligible.

Antitumor Efficacy of PLD Infused by CED

Because 10% PLD was the maximum dose that did

FIG. 1. Tissue sections demonstrating effective distribution of PLD by CED in the normal rodent brain. The 25-μm thick sections obtained at 1-mm intervals were examined with a fluorescence microscope to detect the signals generated from doxorubicin with ultraviolet illumination. Original magnification × 12.5.

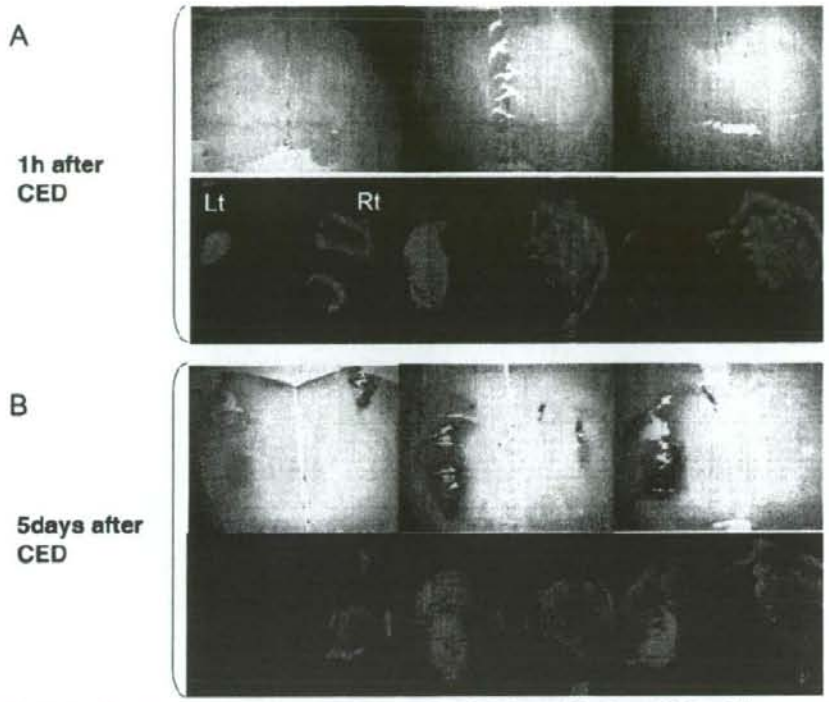

FIG. 2. Light microscopy images (*upper rows* in A and B; original magnification × 12.5) and fluorescence microscopy images detecting fluorescence generated from doxorubicin with ultraviolet illumination (*lower rows* in A and B). Images show tissue distribution of PLD *(right hemisphere)* or free doxorubicin *(left hemisphere)* after CED in 6 rats. Three rats were killed 1 hour after infusion (A) and 3 others were killed 5 days after infusion (B). Three sequential 25-μm sections at 1-mm intervals from a representative rat at each time point are shown.

not cause damage to normal brain tissue, this concentration was used in the survival study (Fig. 5).

Among the rats in the U-251MG xenograft model, those in the sham surgery group that received CED of PBS were all killed 41–45 days after tumor cell implantation because of neurological symptoms indicative of tumor progression. Five of 6 rats that received 0.2 mg/ml doxorubicin as PLD by CED had to be killed 55–67 days after tumor implantation, and 1 rat lived until the end of this study. Formation of large tumors was verified in all rats killed in these groups. The survival of rats that received 0.2 mg/ml doxorubicin as PLD was significantly longer than in rats that underwent mock surgery ($p = 0.0006$, log-rank test).

The U-87MG rats in the mock surgery group were all killed 15 to 16 days after tumor cell implantation because of neurological symptoms indicative of tumor progression. All rats that received 0.2 mg/ml doxorubicin as PLD by CED had to be killed 14–19 days after tumor implantation. Formation of large tumors was verified in all rats killed in these groups. The survival of rats that received 0.2 mg/ml doxorubicin as PLD was significantly

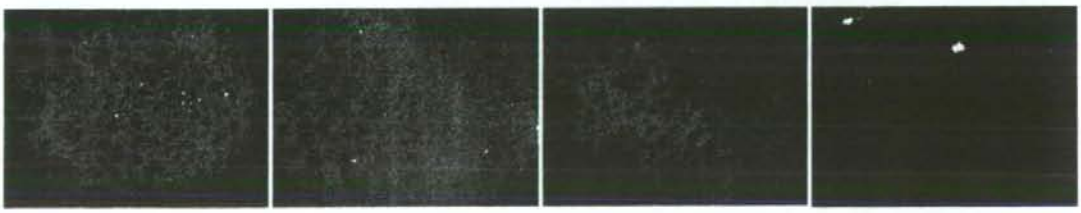

FIG. 3. Fluorescence microscopy demonstrating retention of PLD after CED in the normal rodent brain. Fluorescence was strongly observed for 14 days after infusion but then diminished. Sixty days after infusion, the fluorescence had almost faded away and was hardly detectable. Original magnification × 50.

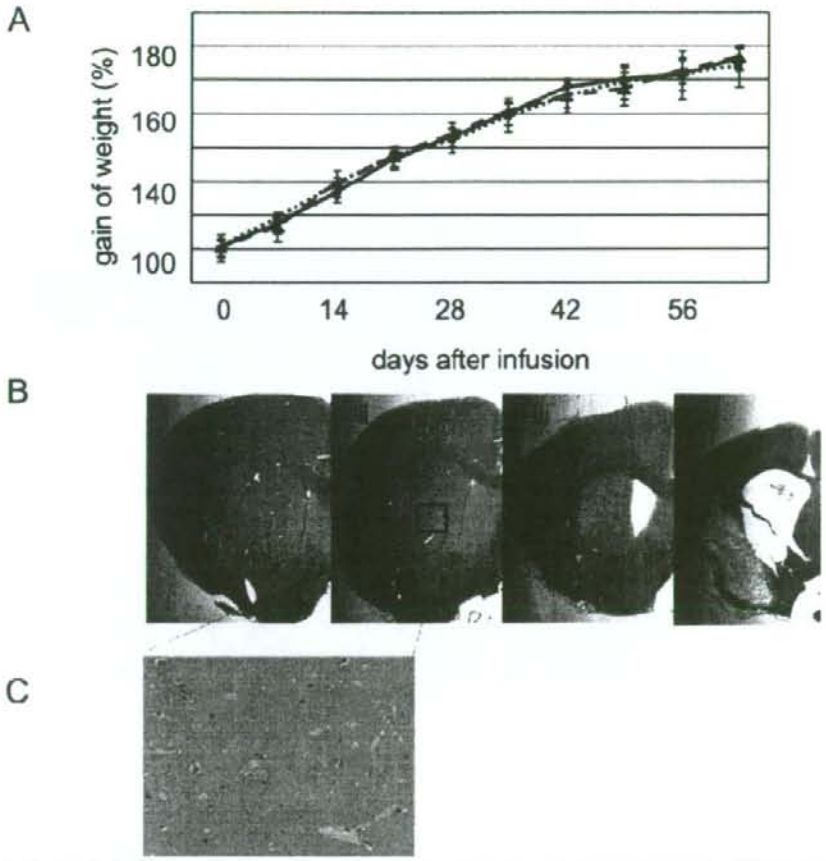

FIG. 4. A: Graph demonstrating weight gain observed during the study period in rats that received PBS *(solid line)*, 10% PLD *(dotted line)*, and 100% PLD *(dashed line)*. The 20% PLD group is not shown. All rats gained weight at the same rate. B: Photomicrographs obtained 63 days after infusion revealing local tissue damage and atrophy of the infused hemisphere in all groups (i, control; ii, 10% PLD; iii, 20% PLD; and iv, 100% PLD). C: Higher magnification photomicrograph of *boxed area*. Original magnification × 12.5 (B) and × 100 (C).

longer than in the mock surgery group ($p = 0.016$, log-rank test).

Discussion

Polyethylene glycol–coated liposomal doxorubicin is formulated with surface-bound polyethylene glycol to protect the liposomes from detection by the monocytes and macrophages in the liver and spleen after systemic delivery. The pharmacokinetics of PLD compared with those of free doxorubicin involve a prolonged circulation time, increased accumulation in the tumor, sustained drug release, and reduced systemic side effects. Intravenous administration of PLD resulted in enhanced drug exposure and improved therapeutic efficacy in a rodent brain glioma model.[15] Intravenous injection of PLD is safe and moderately effective in patients with recurrent high-grade gliomas.[5] Local intratumoral administration of free doxorubicin appeared to be safe and effective in 10 patients suffering high-grade gliomas.[16] Considering these previous data, local administration of PLD may have therapeutic advantages compared with free drug administration.

Convection-enhanced delivery can achieve extensive distribution of the locally applied agents, and CED of liposomal agents with slow-release capability may achieve ideal drug delivery for malignant gliomas. Liposomes were extensively distributed after CED into the brain parenchyma in the present (Fig. 1) and in previous studies.[7,11] The distribution of PLD was more extensive than that of free doxorubicin (Fig. 2). This finding is consistent with our previous observation that free doxorubicin is immediately absorbed in the nuclei, whereas PLD diffuses through the intercellular space, resulting in wider distribution.[14] Free-drug infusion by CED into the striatum damaged the brain more rapidly than PLD infused by CED. A large area of tissue necrosis was observed at